Progress of Ceramic Research in the Shanghai Institute of Ceramics, Academia Sinica

INVITED REVIEW PAPER

TUNG-SHENG YEN
Director, Shanghai Institute of Ceramics, Shanghai, China

Research activities in the Shanghai Institute of Ceramics of the Chinese Academy of Sciences started in the early fifties after the founding of the People's Republic of China. The Institute is now an establishment devoted essentially to studies of inorganic materials with a broad spectrum of research projects relating to single crystal studies, glass (amorphous material) research, oxide and non-oxide ceramics research, ferroics studies, fast-ion conductor research, inorganic coating materials studies and research on ancient Chinese porcelain and glazes. Problems concerned with processing, characterization, microstructure and properties are involved. Other major branches of ceramic science and engineering are being studied in other institutions run by the Building Materials, Light Industries and Metallurgy Departments of the Government and some Universities and Institutions of Technology. This review gives an account of the works that are being carried out in the Shangai Institute. It is, however, not intended to be a complete coverage.

1 - SINGLE CRYSTAL STUDIES

Single crystal studies have been carried out in the Shanghai Institute of Ceramics since the beginning of the sixties. Both single crystal growth as well as physical properties have been studied. Those that have received the more intensive work can be classified into two categories. Single crystals that are naturally available but are either scarce in quantity or are not usually good enough in quality comprise one category. Quartz, mica, and diamond are the three representative materials that have drawn much attention. The new single crystalline materials for high technology applications, such as laser crystals and electro-optic, acousto-optic and nonlinear optic crystals, are another category that forms the second center of interest.

1.1 - Synthetic quartz, mica and diamond research

The study of quartz crystal growth under hydrothermal conditions started in 1958 and reached pilot production stage in 1962. Synthetic quartz is now completely self-sufficient in China for various industrial purposes and has been exported for a number of years. Q-values of the crystals have attained the level of $1.5\text{-}2.5 \times 10^6$, and some have reached the optical quality necessary for lenses (Fig. 1). Some fundamental research has also been pursued in relation to the growth habit and its lattice structural unit. It is postulated that the crystallization habit and defects developed have a close relationship with the simple structural unit of quartz, i.e. the trigonal tripezohedron [1]. It has also been proposed from thermodynamic consideration of interfacial free energy that, statistically speaking, the most probable growth unit is the metastable ring shaped $Si_6O_6(OH)_{12}$ group. In accordance with the structure of the crystal and the orientation of the growing surface, the unit groups will be oriented to adopt the maximum possible molecular reentrant angles so as to mimimize the interfacial free energy [2].

As is known, mica is a layered-structure mineral. The Shanghai Institute of Ceramics started mica single crystal growth in the early sixties. The type of mica studied is fluorophlogopite, $KMg_3(AlSi_3O_{10})F_2$. Due to its complex composition, the melt is easily supercooled. Though a number of attempts have been tried in some countries over the past forty years, good single crystal growth is apparently difficult. The problem that we have tried to attack is to grow large single crystals with high yield and low defect concentrations. Investigations were carried out to study the relationship between melt composition and phases crystallized, the influence of thermal history on supercooling, and the careful determination of the heat of mica crystallization [3]. It was then possible to fix the proper composition limit, to choose a suitable thermal environment, as well as the maximum growth rate with well aligned seed crystals under a specified temperature field to have good crystals grown. The essence of the processing parameters is to establish a most exact temperature profile across the melt and to realize a most careful temperature control throughout the whole growth period. Using the crucible lowering technique (Bridgeman method) and introducing seed crystal at the bottom part, at present large mica crystals of $\sim 100 \times 100$ mm in size can be grown in

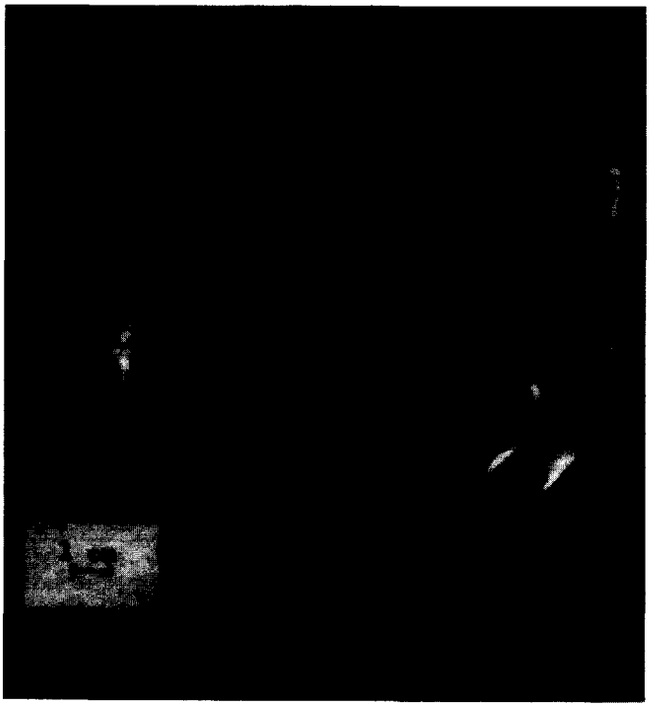

FIGURE 1 - Large quartz crystal grown hydrothermaly.

TABLE I - Some properties of synthetic as compared to natural mica.

	Natural muscovite (szechuan province) china	Synthetic fluorophlogopite (this laboratory)
Max. temperature usable, °C	600	1000
Coef. thermal expansion, /°C (20-800°C)	—	8.8×10^{-6}
Light transmission, % (λ = 0.4-4.5 μm, specimen thickness ≃ 0.2 mm)	80 strong absorption at 1.4 and 2.8 μm	~92
Compression strength, MN/m² (⊥ cleavage plane)	710	520
Tensile strength, MN/m² (// cleavage plane)	504	514
Dielectric constant, ε (16-600°C)		
1 KC	7.5-6.7	5.3-5.7
1 MC	6.8	5.7
Loss factor, tg δ, 20°C		
1 KC	6.8×10^{-4}	5.0×10^{-4}
1 MC	9.8×10^{-4}	2.0×10^{-4}
Volume resistivity, ρ v, Ω · cm		
Room temp.	3.8×10^{15}	2.7×10^{16}
100°C	3.5×10^{15}	2.5×10^{16}
200°C	3.5×10^{14}	2.0×10^{16}
300°C	1.4×10^{13}	3.5×10^{15}
600°C	2.0×10^{9}	5.0×10^{12}
Dielectric strength, KV/mm (⊥ cleavage plane, sample thickness, 10-50 μm)	221-87	192-94

brooklet form of 10-15 mm thickness, which can be cleaved into very thin sheets of almost perfect appearance (Figs. 2 and 3). These synthetic mica crystals have been shown to have better transparency, be able to stand much higher temperature without decomposition and to have similar or better electrical properties as compared with natural mica minerals. Some of the properties are compared in Table I.

These synthetic mica materials have already been used in electronic tubes, capacitors, and as various window materials [4].

The formation and morphology of defects in large sheet mica crystals have been studied by Lang's X-ray topography and other techniques [5]. Growth striations, twinning, crystal basal face corrugation and other defects are common. It is postulated that these defects are mainly originated from the seed crystals and/or are due to the occurrence of an improper temperature profile during the growth period.

The research on synthetic diamond has attracted investigators of this Institute both from the practical point of view and also as a study of crystal growth under high temperature and very high pressure conditions. The first high pressure apparatus of 300 ton capacity was designed and built in 1962 with 6 anvils driven simultaneously by one power source. We call it an unidirectionally loaded four-paired sliding-face cubic ultra-high pressure apparatus [6]. Thereafter a 1000 ton and another 5000 ton capacity press were successively built in 1969 and 1976 respectively (Figs. 4 and 5). Experiments carried out in these set-ups through these years did show very good synchronization in performance and it was also rather steady in pressure maintenance.

Works that have been carried out include: (1) the establishment and maintenance of specific temperature and pressure gradients suitable for the growth of diamond grains of different sizes; (2) the study of the effect of the metal catalysts used on the growth of diamond; and (3) the nucleation and growth of large

FIGURE 2 - Synthetic fluorophlogopite in booket form which can be cleaved.

FIGURE 3 - Cleaved thin sheet synthetic mica with almost perfect appearance.

FIGURE 4 - A 5000 ton capacity press with its control panels.

FIGURE 5 - Close up of the 5000 ton press showing the ultra-high pressure apparatus in position.

diamond single crystals in the graphite-diamond system by the thin metal-film method.

Under a proper temperature and pressure field, graphite dissolves in the molten metal and diffuses to the other side where diamond nucleates. A molten metal thin-film separates the graphite-diamond interface. Accompanying the growth of diamond crystal, the metal thin-film is pushed outward and the diamond grows by an automatically moving thin-film solvent mechanism [7]. Bq this way, we can now grow diamond crystals of about 1.5-2 mm size with reasonably good quality (Figs. 6 and 7). We are also growing coarse grained abrasive

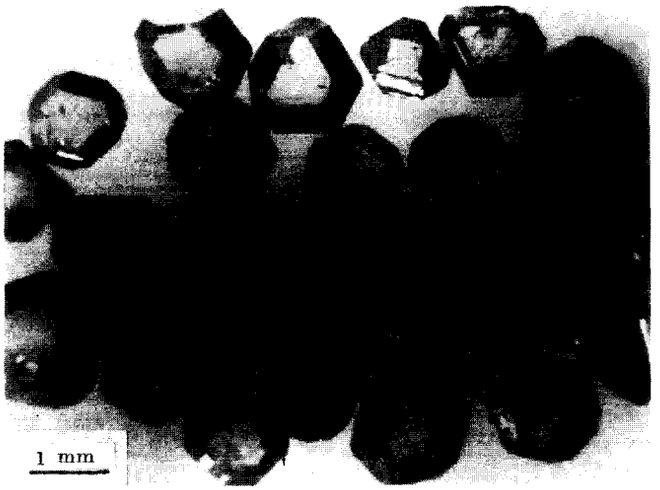

FIGURE 6 - Medium sized diamond single crystals with rather perfect octahedral morphology.

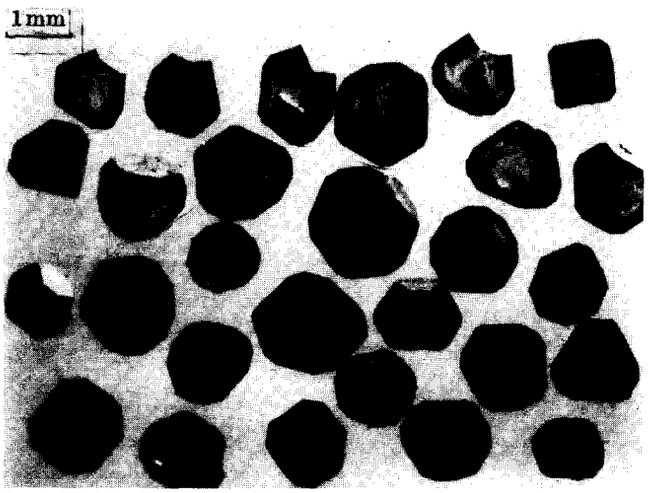

FIGURE 7 - Diamond single crystals synthesized with rather perfect cubo-octahadral growth morphology.

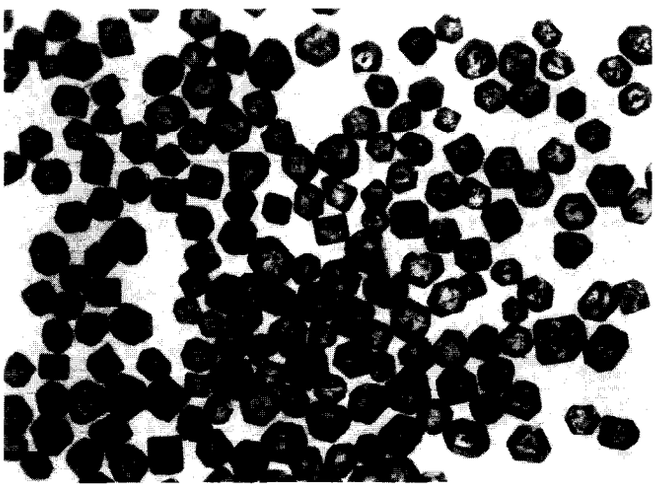

FIGURE 8 - Coarse grained diamond crystals synthesized.

grade diamond aiming at a better yield by changing the temperature gradient in the high-pressure cavity (Fig. 8). These works are still in progress to get a better idea of the mechanism of diamond growth and to find better ways of maintaining the reproducible temperature and pressure environments which are required for these different growth purposes.

1.2 - Laser crystal and non-linear optical crystal studies

Since 1959 several Institutes in China have started research on the growth of laser ruby crystals by the Verneil method. The first ruby laser was developed in our country in 1961. By the mid-sixties, the Shanghai Institute of Ceramics had mastered the technique of growing long ruby boules of fairly good quality. Laser rods up to 1 m in length and over 2 cm in diameter were used in laser operations, the output of which reached 3000 joules per pulse. Later, this technique of growing ruby was transferred and developed at the Jao-zhuo Institute of Laser Technology. Laser ruby crystals are now grown with even better quality. The average lasing efficiency is around 0.8% and the best values can be as high as 1.7%.

Starting from the mid-seventies, a variety of electro-optic and non-linear optic crystals for laser technology, such as lithium niobate (LN), lithium tantalate (LT), and barium sodium niobate, and acousto-optic crystals, such as lead molybdate and tellurium oxide, have been grown from the melt by the Czochralski method (Figs. 9, 10).

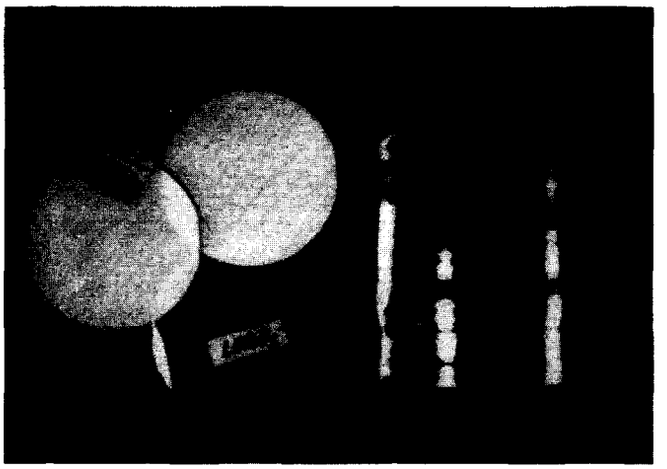

FIGURE 9 - Lithium niobate and other electro-optical crystals grown.

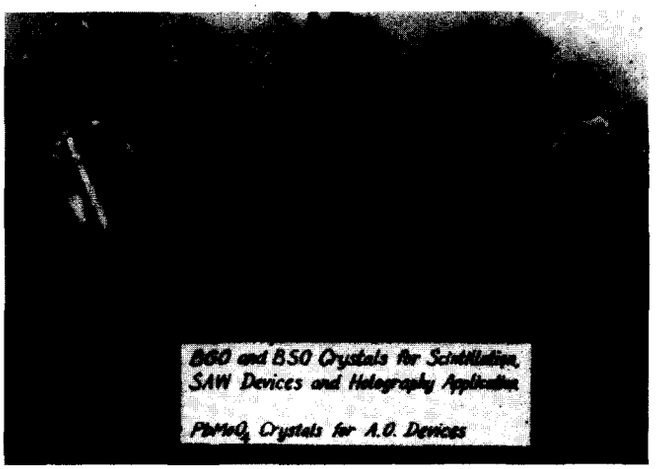

FIGURE 10 - Lead molybdate and other acousto-optical crystals grown.

The growth mechanisms and the optimization of parameters suitable for the growth of crystals having high optical uniformity have been studied. For instance, for the growth of high quality LN single crystals, the temperature field across the melt surface is of the utmost importance [8]. It is found that, in general, the temperature gradient in the gaseous phase just above the melt line

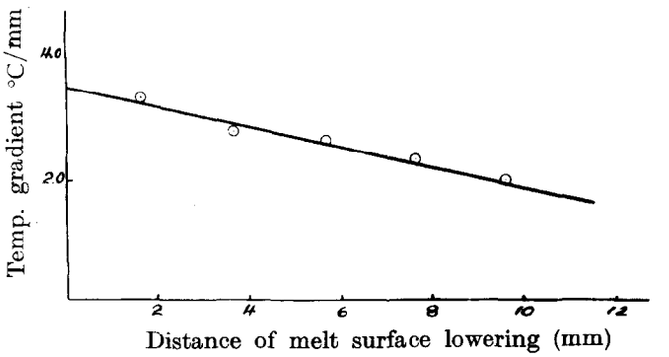

FIGURE 11 - The temperature gradient near the Crystal-Melt interface as a function of the lowering of the melt surface.

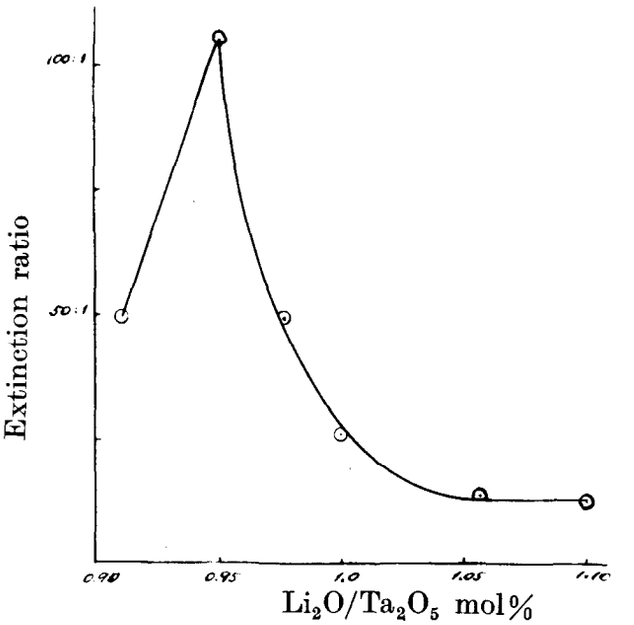

FIGURE 12 - Extinction ratio of $LiTaO_3$ vs. Li_2O/Ta_2O_5 ratio.

decreases with the lowering of the melt surface and that the temperature of the surface of the melt increases (Fig. 11). It is therefore essential to adjust the static temperature profile during growth so as to keep a good environment for the dissipation of latent heat.

For lithium tantalate, we have determined the congruent melting composition to be near Li/Ta = 0.95 atom ratio [9]. It is important to keep the melt composition as close to this ratio as possible to get crystals of good optical uniformity. Crystals with low birefringence gradient (of the order of 10^{-5}/cm and with a minimum value of $\sim 1.3 \times 10^{-5}$/cm) can be obtained in this laboratory. The extinction ratio of the crystals can also be kept at better than 100:1, with a maximum of about 375:1. Still better results can be obtained with purer raw materials (Fig. 12). At a Li/Ta atomic ratio of 1.08, a new phase, Li_3TaO_4, appears and the extinction ratio of the crystal drops to a minimum. The optical uniformity of crystals grown from melts of varying composition fits closely with the data obtained from phase equilibrium studies.

The loss factor of the LT crystals grown is related to their chemical composition, the growth parameters used, and the conditions of annealing and poling treatments [10]. It has been identified that crystals grown normal to the (1011) lattice plane have the best pyroelectric properties and have a loss factor, $\tan\delta$, of 4×10^{-4}. Pyroelectric detectors have been studied with either lithium tantalate or strontium barium niobate crystals.

1.3 - Some crystal physics studies

In the field of crystal physics, we have a group of people working on optical and electrical property characterization. The crystal defects and other factors that influence the electro-optic, acousto-optic, second harmonic generation (SHG), holographic storage and pyroelectric effects are also being investigated. In relation to the electro-optic effect of lithium niobate, it is found that certain environmental factors, for instance, temperature variation, light radiation, or the condensation of charged particles in the ambient atmosphere will change the surface charge condition of the sample and thus affect the extinction ratio of the electro-optic modulator [11]. Means have been found and adopted to alleviate such effects. Electro-optic modulators of LN have already been used in a dual frequency He-Ne laser with frequency stabilization and also in a He-Ne laser with power stabilization.

Studies on lead molybdate single crystals and devices have resulted in acousto-optic modulators with low driven power and high diffraction efficiency [12]. With less than 0.5 watt driven power, a diffraction efficiency of better than 70% can be obtained from lead molybdate acousto-optic modulators of central frequency 50-90 MHz.

TABLE II - Lead molybdade acousto-optic modulator.

Diffraction efficiency	>80%
Driven power	0.5 W
Bandwidth	15 MHz
Transmission	>85%
Aperture	1 mm
Impedance	50 Ω
Central frequency	70 MHz

SHG devices of barium sodium niobate with an output power of 0.53 μm green light up to or better than the 1 watt level has been achieved through the up grading of the purity of the crystal the improvement of the detwinning technique, as well as through the control of the phase-matching conditions [13]. The conversion efficiency can be as high as 70% (Fig. 13). These results are rather new and are probably not yet reached in the open literature.

We have also studied the holographic storage properties of doped strontium barium niobate in relation to the crystal composition, the level of doping, and the lattice orientation selected [14]. Using the 100 plane for storage, a diffraction efficiency of >90% has been obtained. The exposure level at 10% diffraction efficiency amounts to only 14 mJ/cm^2, which is about 1-2 order of magnitude more sensitive than for doped lithium niobate. Only a He-Ne laser is needed to write in, read out or to erase.

2 - GLASS RESEARCH

In the field of glass research, a number of projects have been carried out.

2.1 - Glass ceramic material research

We started research on glass ceramic materials in the late firties; since then, many oxide systems have been investigated, including both optically induced and thermally induced nucleation systems. Considerable attention has been paid to nucleation and crystallization phenomena. The effect of thermal history on the final microstructure and properties of certain glass-ceramic systems is very interesting [15]. We have studied MgO-

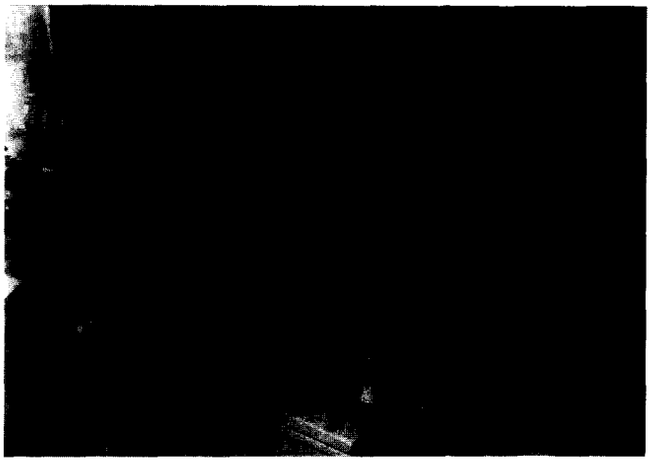

FIGURE 13 - SHG effect of barium sodium niobate with 0.53 μm output power greater than 1 watt.

FIGURE 14 - Microstructure of MgO-Al$_2$O$_3$-SiO$_2$ system glass ceramics (sample A) after thermal treatment at 650°C, SEM.

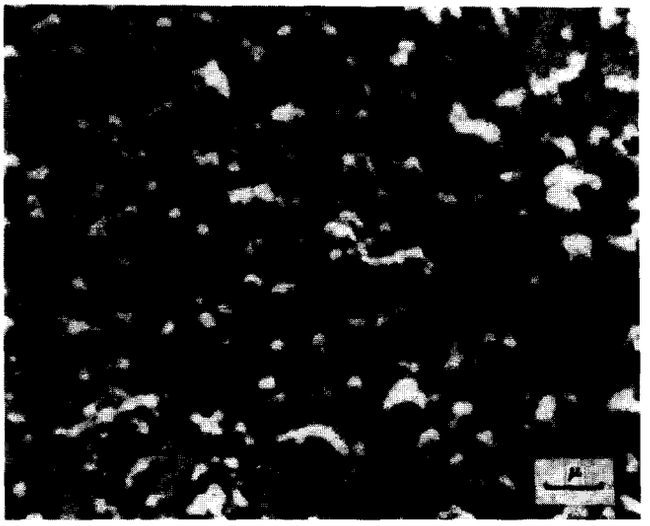

FIGURE 15 - Microstructure of MgO-Al_2O_3-SiO_2 system glass ceramics (sample B) after thermal treatment at 750°C, SEM.

Al_2O_3-SiO_2 glass-ceramics near the cordierite composition using TiO_2 as the nucleating agent. We found that thermal treatment at lower temperature caused phase separation or spinodal decomposition of these compositions (Figs. 14, 15). A different thermal history resulted in quite different crystallization sequences. A similar glass composition when pretreated at 650 and 750°C

FIGURE 16 - Microstructure of glass ceramics of 650°C pretreated and 1250°C crystallized material (X 138).

FIGURE 17 - Microstructure of glass ceramics of 750°C pretreated and 1250°C crystallized material (X 138).

respectively showed very different crystallization paths during later high temperature treatments. Although the finel crystalline phases were all similar (composed mainly of α-cordierite, MgAl titanate and rutile), they have quite different microstructures due apparently to the different sequences of crystallization (Figs. 16, 17). An interesting thing that follows is that they have very different properties. The numerous microcracks in the second sample (Fig. 17) lowered its mechanical strength but enhanced greatly its thermal shock resistance which may develop into a very useful property. Its much enhanced thermal shock behavior may go in parallel with much better fracture toughness which may be worthwhile for further study.

TABLE III - Properties of the same composition of glass-ceramic but with different thermal history.

Pretreatment condition	Properties after final crystallization treatment		
	MOR MN/m^2	Thermal exp. coef. (0-600°C) $\times 10^7/°C$	Remanent str. after quenching from 500°C to water at room temp. MN/m^2
a, 650°C	150-170	19-21	cracked
b, 750°C	40-55	8-12	43

2.2 - Glass fiber optical waveguide material research

Fiber glass optical waveguide materials with multimode graded indices have been prepared specifically by the CVD method. The processing parameters to obtain low loss, and suitable refractive index distribution which means high transmission capacity waveguide fibers have been pursued. For instance, the SiO_2-P_2O_5 system has been studied in detail [16], and a refractive index distribution profile like that of Figure 18 can be obtained rather reproducibly. The widening of the input pulse after passing through a fiber of about one Km distance is <0.5 ns and the band width is >500 MHz/Km. The total loss of the fiber is about 2-4 dB/Km (at 0.85 μm) with an average strength of 4-5 GN/m^2 and a Weibull modulus of 7-9. Production units in Shanghai have already been established on this basis. A 1.8 Km optical transmission cable has been used experimentally for more than two years and has been integrated into the municipal telephone network.

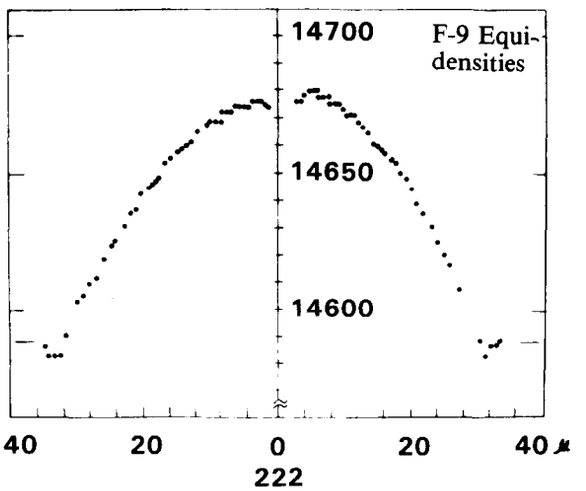

FIGURE 18 - Typical refractive index profile of fiber waveguide with P_2O_5-SiO_2 system prepared by CVD.

2.3 - Amorphous semiconducting material studies

With the chalcogenide series of amorphous semiconducting materials, by the use of the reversible amorphous ⇌ crystalline transformation under an electric pulse, we have studied systematically the relationship between composition, crystallization behavior and electrical properties [17]. The composition range suitable for fabricating an EROM (erasable read only memory) has been found to be the following:

TABLE IV - Composition range for EROM.

Te	83-75 atom percent
Ge	13-21 atom percent
S	1-2 atom percent
Sb (or Bi)	2 atom percent

8 x 8 EROM device can be made on chips of 1.3 x 1.0 mm^2 size with characteristics as shown in Table V.

For devices to be operated at higher temperatures, it is essential to increase the transformation temperature T_g and the crystallization temperature T_x of the amorphous materials. This can be achieved by increasing the Ge content owing to its ability to increase the amount of cross-linked bonds, thus enhancing the rigidity

TABLE V - Characteristics of chalcogenide EROM device.

Read out speed	2-10 ns
Read out life	$>10^{12}$
High resistance state	$2 \times 10^{4}\ \Omega$ cm
Low resistance state	$2 \times 10^{-1}\ \Omega$ cm
Write-erase cycle	$>10^{5}$
Operative temperature	—50° - - +60°C

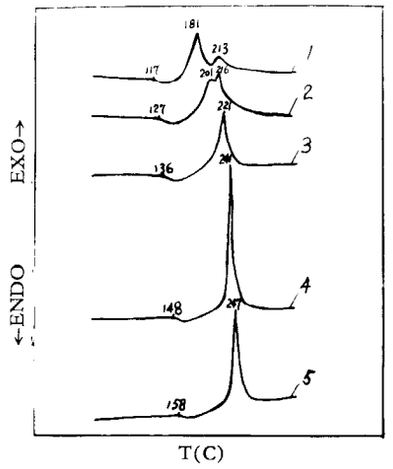

FIGURE 19 - Differential scanning calorimetry (DSC) curves of chalcogenide glasses with different Te/Ge ratios.

of the structure [18]. Chalcogenide glasses with varying Te/Ge ratios show a range of T_g from 117-158°C, and T_x from 181-247°C (Fig. 19).

The influence of a minor amount of additives on the phenomena of phase separation, crystallization and thence on the stability and life time of the devices has also been studied in some detail.

The action of light on the change of optical and electrical properties of certain thin film chalcogenide glasses is also of practical and theoretical interest. Various types of compositions have been studied for their holographic storage properties and recently as xerographic photoconductors as well as photoconductive target materials for TV cameras.

For optical storage, thin films with a composition essentially of As_2S_3 have been studied in detail for their processing parameters and properties [19]. Resolution of 2600 lines/mm and diffraction efficiency of better than 40% can be obtained consistently on large sized films which might be extremely valuable for high information storage density purposes. This may be particularly useful for the storage of Chinese characters which are many thousands in number and each of which comprises a huge volume of information. Figure 20 is the display of a stored spot of about one millimeter size. You can see the amount of information stored in it.

Lately, we have studied the optical and photoelectrical properties of these types of material in some depth [20]. For instance, the photo-induced optical properties of these thin films change dynamically under different thermal treatments which thus affect their holographic storage behaviour. The dynamic change of optical path (nd) was used as a measure to study the change of structure of the glassy phase. It can be seen (Fig. 21) that the structure change with time at temperatures below the T_g point first follows a first order rate process and then slows down. This relates

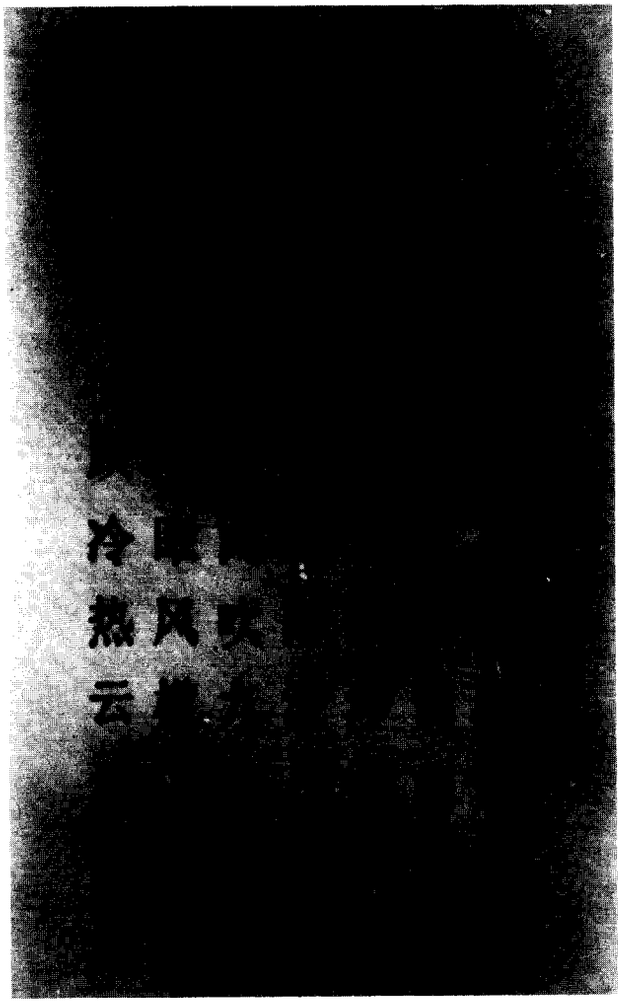

FIGURE 20 - Information optically stored in a spot of chalcogenide glass medium and displayed by He-Ne laser.

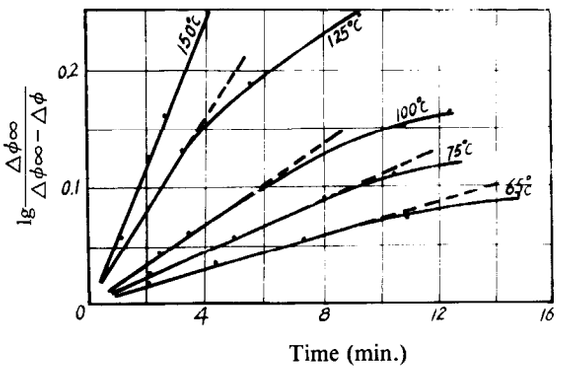

FIGURE 21 - The change of $\Delta\phi$ with time when as deposited As_2S_3 film is treated at different temperatures.

probably with the numerous kinds of « misfit bonds », « dangling bonds », or other « defects » present in the amorphous film. After having gone through a certain thermal history, the optically induced change of (nd) decreases. The higher the temperature of thermal treatment the greater the deteriorating effect (Fig. 22). This explains the basis of environmental influence on holographic storage properties (difficult to write in and with lower diffraction efficiencies).

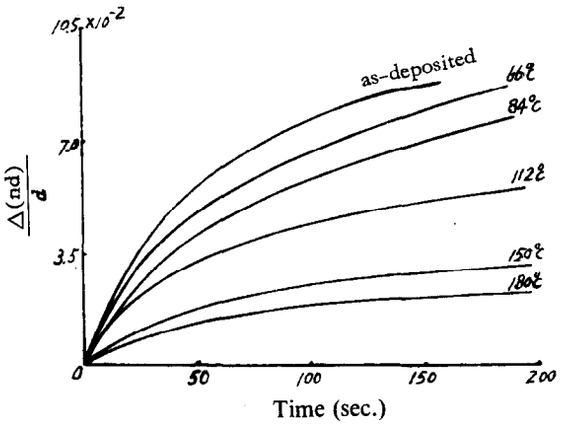

FIGURE 22 - The dynamic process of optically induced optical path change of As_2S_3 film after different heat treatment conditions.

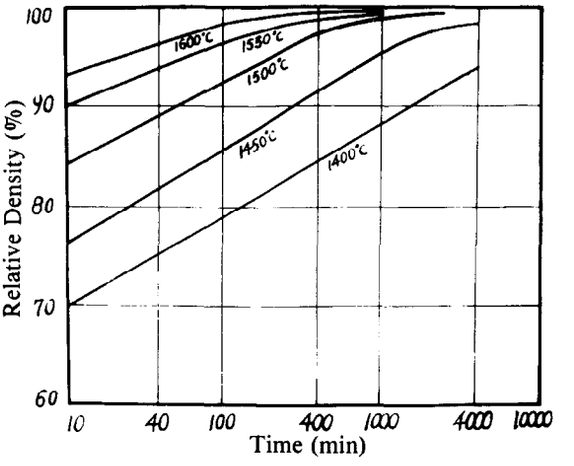

FIGURE 23 - The change of density vs time when α-Al_2O_3 is sintered at constant temperature.

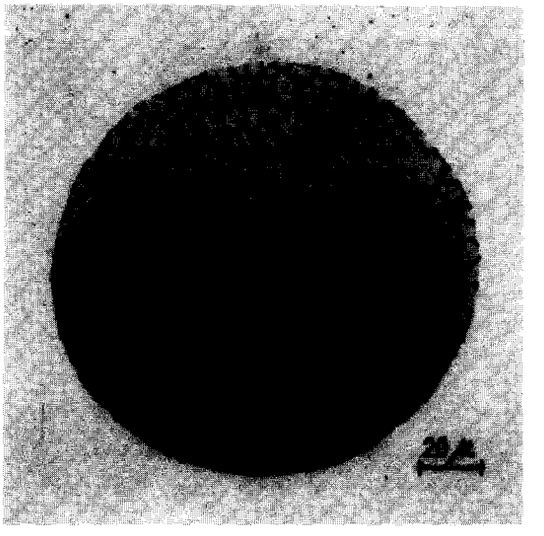

FIGURE 24 - Microstructure of sintered Al_2O_3 close to theoretical density with MgO additive.

3 - OXIDE AND NON-OXIDE CERAMICS RESEARCH

3.1 - Oxide ceramics processing research

We started our processing and fabrication research on alumina ceramics in the early fifties, then expanded our program to include zirconia, magnesia, calcia, and beryllia from the late fifties through the sixties. These results helped the later development into industrial production of such materials in a number of factories in China.

In the processing study of alumina, we started to use MgO as additive in 1955 and got microcrystalline materials with a bulk density of 3.90, which is about 98% of the theoretical density [21]. They are suitable as cutting tool bits and perform satisfactorily in certain applications. They have a jade like appearance but are not really semi-transparent. The real credit of rendering alumina practically pore free and semi-transparent which has a density close to its theoretical value, should go to Professor Coble [22, 23]. The operative mechanism of the additive in promoting sintering and pore removal has been a problem of debate over the last twenty years. We, however, succeeded in sintering alumina close to its theoretical density at temperatures as low as 1550-1600°C in the early sixties (Fig. 23) [24]. Using pure α-Al_2O_3 as the starting material with a specific surface area of about 5-8 m^2/g and adding MgO at the level of 500 ppm as the sintering aid, we first succeeded in China in sintering Al_2O_3 to good semi-transparency in the midsixties. The total light transmittance from tubing made out of this material amounted to 90-92%, and high-pressure Na vapor lamps were first made in China around that time. The microstructure of that material is almost pore free (Fig. 24). As is shown in Table VI, with the increase in the level of MgO dopant, the average grain sizes of the sintered material decrease while the in-line light transmittance values decrease. This is in accord with the modern understanding of the role of magnesia additive in sintering and grain growth. At an increasing level of MgO addition, besides pore drag and/or solid solution drag which retard grain growth, there is an additional pinning effect of secondary phase at the grain boundaries. But as to in-line light transmittance, both grain size decrease and the presence of increasing amount of second phase at the grain boundary will enhance scattering and decrease transmittance.

3.2 - Non-oxide powder preparation studies

For the processing and fabrication of Si_3N_4 and SiC ceramics, the characteristics of the starting material are of paramount importance. Besides using powdery materials of Si_3N_4 and SiC prepared by ordinary means, we also tried to find new ways of preparing fine, uniformly sized Si_3N_4 and SiC materials by the reduction of SiO_2.

3.2.1 - Submicron Si_3N_4 material preparation [25]

Starting out from high purity colloidal SiO_2 and carbon black with specific surfaces of 360 m^2/g and 165 m^2/g respectively, Si_3N_4 was synthesized by the overall reaction:

$$3SiO_2 + 6C + 2N_2 = Si_3N_4 + 6CO$$

TABLE VI - The influence on grain size and in-line transmittance of sintered Al_2O_3 with MgO additive level and sintering temperature.

MgO additive % content,	Sintering condition (H_2 atm)	Av grain size μm In-line	transmittance * 2 μm	5 μm
0.1	1600-10 hr	9	4.5%	23%
0.1	1700-10 hr	13	25%	53%
0.1	1800-10 hr	38	57%	74%
0.15	1600-10 hr	7	3 %	7 %
0.15	1700-10 hr	11	8 %	28%
0.15	1800-9 hr	18	32%	53%

* Sample thickness = 0.8 mm.

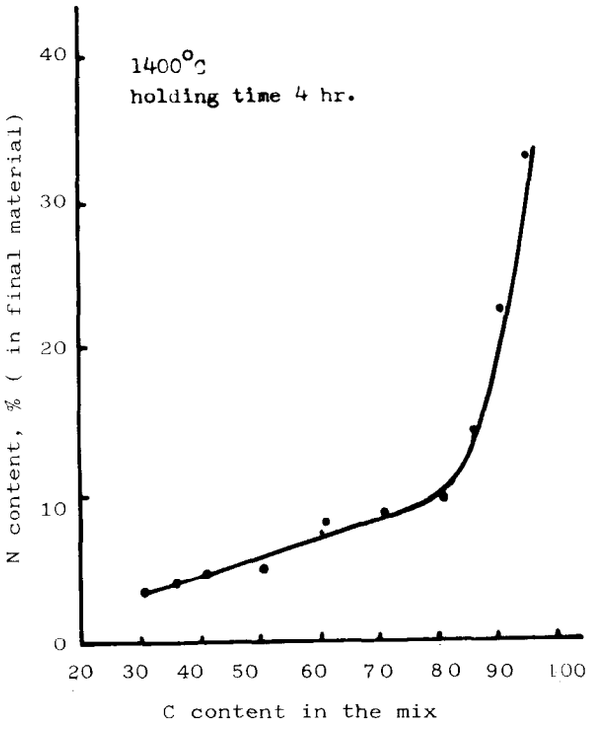

FIGURE 25 - The degree of nitridation with different C content in the mix.

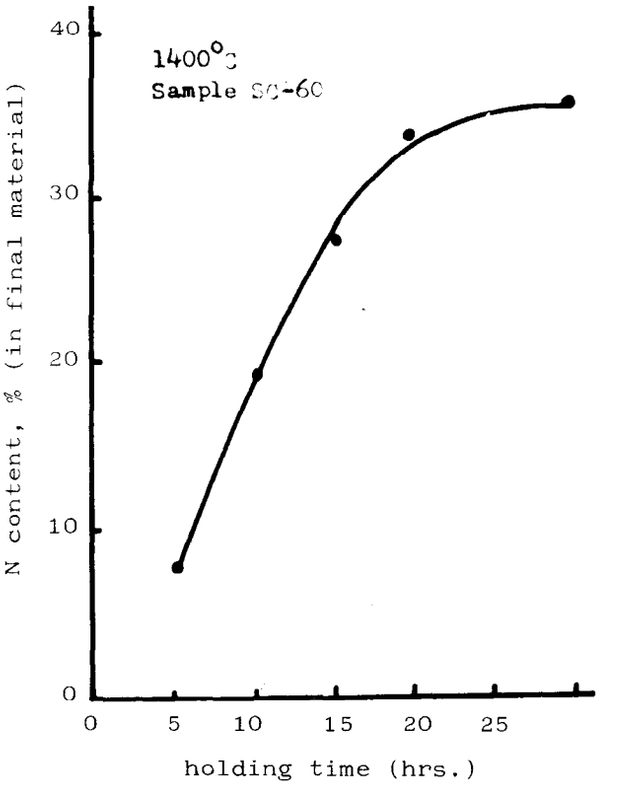

FIGURE 26 - The degree of nitridation with increasing holding time.

Experiments showed that the degree of nitridation increased with temperature, with increasing C content in the mix (Fig. 25), and with the time of holding at the max. temperature (Fig. 26). As can be seen from Fig. 25, the silicon nitridation level increased drastically when the C content in the mix was increased beyond 80%. This, in a way, is of course impractical, because the excess C will have to be removed afterwards and the yield will be too low. With an increase in temperature beyond 1400°C, there was also an undesirable side effect, namely the simultaneous formation of SiC in increasing amounts. By increasing the holding time at say 1400°C, the increase in nitridation degree is encouraging (see Fig. 26), but unfortunately the grain size of the Si_3N_4 powder obtained also increases significantly (Fig. 27).

It was found in our experiments that it was possible to increase the degree of nitridation by adding a small amount of some appropriate catalysts and yet the resultant Si_3N_4 powder obtained was submicron in size (Fig. 28). It can be seen that the grain size is quite uniform and is generally less than 0.5 μm.

At present Si_3N_4 powders can be consistently synthesized with a N content >37%, O content <3%, total C ~1% and grain size ~0.5 μm. The remaining problem is to further decrease the total oxygen content.

3.2.2 - High purity submicron β-SiC material preparation [26]

Using high purity colloidal silica and carbon black, each with a total impurity content of <1000 ppm, as starting material, β-SiC was synthesized through the direct reaction:

$$SiO_2 + 3C = SiC + 2CO$$

After optimizing the raw material ratio, and the processing parameters, the above stated reaction could be controlled to proceed practically to completion. Carbon in slight excess which was intentionally added could be removed by post-synthesis calcination. And the free carbon content can be lowered to a level of 0.4%. The characteristics of β-SiC synthesized with a SiO_2/C weight ratio of 60:40 at 1450°C for 4 hrs under a flowing argon stream are summarized in Table VII. The powdery material was decarburized at a temperature of 650°C and its electron micrograph is shown in Fig. 29.

FIGURE 27 - Electron micrograph of Si_3N_4 powder after 20 hr nitridation.

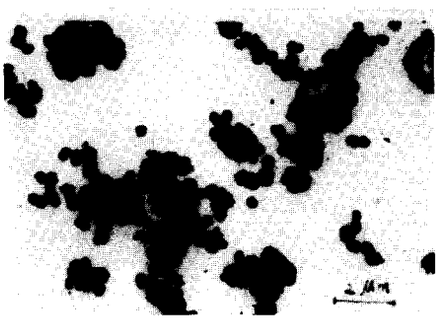

FIGURE 28 - Electron micrograph of Si_3N_4 powder synthesized with a catalyst.

FIGURE 29 - Electron micrograph of β-SiC synthesized.

TABLE VII - Characteristics of submicron β-SiC synthesized.

X-ray analysis	β-SiC
Composition	
By chemical analysis, total Si, %	68.5
free C, %	0.24-0.4
total O_2, %	0.91-1.20
Spectroscopic analysis, impurities in traces	Al, Fe, Ca, Mg
Av. grain size, μm	0.05-0.1
Specific surface area, m^2/g	14-18
Color	yellow

3.3 - Non-oxide ceramics fabrication research

From the beginning of the seventies, we have set about research on non-oxide ceramics. Studies have been carried out on reaction-sintered, hot-pressed and pressureless-sintered Si_3N_4, sintered and hot-pressed SiC and hot-pressed and CVD BN materials.

3.3.1 - Reaction-bonded Si_3N_4 materials fabrication studies

For the processing and fabrication of RBSN material, colleagues in our institute have made detailed studies of the nitridation parameters and evaluated their influence on the microstructure and properties of the materials obtained [27]. RBSN materials and parts are now developed and produced in several factories in China. Some of the samples are shown in Fig. 30. They have found applications as rotating seals and fittings for pumps handling acids, bases and other corrosive and/or abrasive materials with excellent performance. They also perform satisfactorily as parts handling molten aluminum and in other applications.

3.3.2 - Hot-pressed Si_3N_4 material fabrication studies [28]

Hot-pressed Si_3N_4 with MgO or Y_2O_3 and Al_2O_3 as additives has also been studied in some detail. Magnesia as sintering aid for hot-pressing Si_3N_4 has, of course, been extensively studied and reported in the literature. The results we obtained, however, have helped to build

FIGURE 30 - Samples of reaction sintered and hot-pressed Si_3N_4.

up our own production capability in China. The general properties of hot-pressed Si_3N_4 doped with MgO are compared with RBSN in Table VIII. The influence of processing parameters on the degree of densification, $\alpha \rightarrow \beta$ transformation, and mechanical strength is shown in Fig. 31.

The use of Y_2O_3 as sintering aid instead of MgO is meant to enhance the high temperature mechanical properties of hot-pressed Si_3N_4. The simultaneous addition of Al_2O_3 is further meant to lower the first liquid formation temperature thus facilitating full densification of the material at reasonable hot-pressing temperatures. After considerable experimentation, we have chosen a lower level of dopant addition [29]. The gain in mechanical strength of this type of material in comparison with the MgO dopant type is shown in Table IX. The advantages of recrystallizing the grain boundary glassy phase through post-sintering heat treatment are also very encouraging.

Transmission electron microscopy [30] of the hot-pressed material (Y_2O_3 + Al_2O_3 additive) clearly shows its microstructure (Fig. 32). The β'-Si_3N_4 grains are well developed with grain sizes of about 0.3-1.2 μm. The slight expansion of the lattice parameters indicates that some Al_2O_3 has gone into solid solution. Glassy phase exists at multigrain boundaries, and EDXS (energy-dispersive X-ray analysis) shows that there are more impurities

TABLE VIII - Some physical properties of Si_3N_4.

Properties / Material	RBSN	Hot-pressed Si_3N_4 (MgO dopant)
Bulk density, g/cm^3	2.4-2.7	3.26
App. porosity, %	13-18	1
Bending strength, MN/m^2	210-270	750-820
Impact strength, kg-cm/cm^2	1.5-2.0	4
Young modulus, MN/m^2	1.6×10^5	3.0×10^5
Modulus of rigidity, MN/m^2	0.65×10^5	1.2×10^5
Poisson's ratio	0.23	0.23
Hardness, RA	81-85	91-92
Coefficient of thermal expansion, ($\times 10^6$/°C)	2.53 (R.T.-600°C)	2.95 (R.T.-1200°C)
Thermal diffusivity coef., cm^2/sec.	0.0298 (706°C) 0.0272 (850°C)	0.0656 (710°C) 0.0577 (840°C)
Dielectric constant, ε	8.3	4.02
Dielectric loss, tg.δ	0.09	0.02-0.03
Oxidation resistance, wt increase 1400°C mg/cm^2,	2.64 (2 hrs)	2.23 (10 hrs)

TABLE IX - Comparison of bend strength of hot-pressed Si_3N_4 with Y_2O_3 and Al_2O_3 or MgO additives.

Bend strength / Material	H.P. Si_3N_4 with $Y_2O_3+Al_2O_3$ additive	H.P. Si_3N_4 with MgO additive
As hot-pressed material, (1750°C, 30-120 min)		
R.T. bend strength, MN/m^2	820-850	750-820
1000°C, bend strength, MN/m^2	800	710
1200°C, bend strength, MN/m^2	720	560
1300°C, bend strength, MN/m^2	540	440
After recrystallization of G.B. glassy phase		
1000°C, bend strength, MN/m^2	790	—
1200°C, bend strength, MN/m^2	770	—
1300°C, bend strength, MN/m^2	610	—

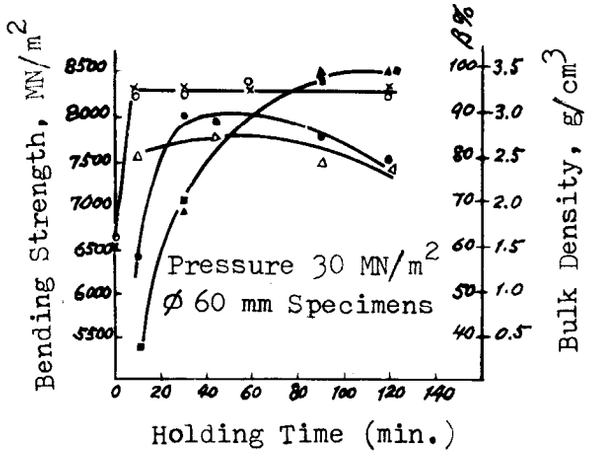

FIGURE 31 - Influence of processing parameters on Si_3N_4 densification, α-β transformation and mechanical strength.
▲ - 1800°C, β % ● - 1750°C, density △ - 1800°C, strength
X - 1800°C, density ● - 1750°C, strength ■ - 1750°C, β %

in these areas (Ca, Si, Ti, Fe). By means of the bright field electron microscopy technique, the thin layers of glassy phase around the crystalline grains can be clearly seen (Fig. 33).

After heat treatment of the as-pressed materials at temperatures of 1200-1400°C, TEM studies also show the appearance of new phases containing Y and N at the grain boundaries and the evident decrease of the quantity of the glassy phase. The crystallization of the grain boundary glassy phase by heat treatment has also been clearly shown by thermal diffusivity and thermal conductivity studies of the materials [31].

3.3.3 - The processing of Si_3N_4 at super-high pressures without an additive

We tried to hot press Si_3N_4 (90-95% α-phase) using our high pressureset up to super-high pressures without adding any sintering aid to see how densification goes [32]. We found that samples with Φ 5 x 6 mm size could be well sintered at 54 kilobar pressure and 1750°C. At 54 kilobar pressure and 1350°C, the sample could also be densified to similar bulk density, but the crystalline grains remained essentially in the α-form. No phase transformation appeared. A comparison of some of the properties with ordinary hot-pressed Si_3N_4 (with MgO additive) is shown in Table X).

FIGURE 32 - Electron micrograph of H.P. Si_3N_4 - area 1, glassy phase at multi-grain junctions; area 2, glassy phase completely enveloped by β'-Si_3N_4 grains.

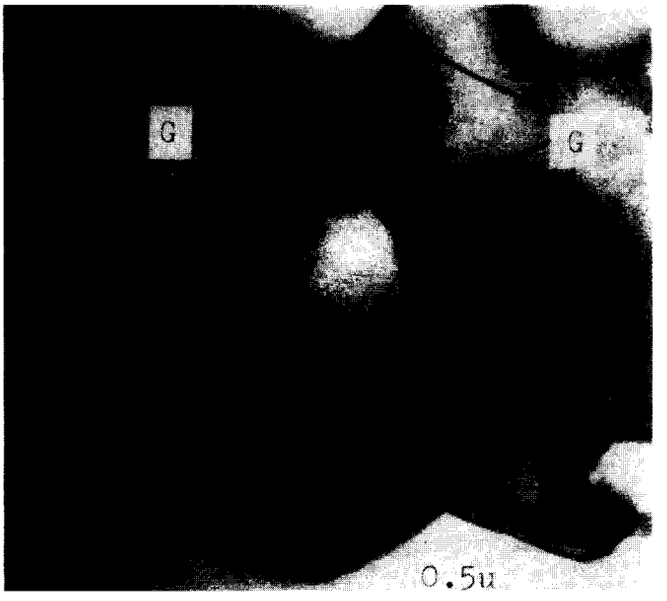

FIGURE 33 - Bright field micrcgraph showing the glassy phase at the grain boundaries.

4 - PIEZOELECTRIC AND FERROELECTRIC MATERIALS RESEARCH

In the electronic ceramics laboratory, our attentions have been concentrated on ferroelectric and piezoelectric materials studies, including barium titanate, magnesium lanthanum titanate, various niobates, and especially lead zirconate titanate ceramics. For the latter, studies have been carried out particularly on the correlation between composition, additives and their piezoelectric properties [33]. As a result of these studies, materials having different piezoelectric parameters have been obtained that are suitable for use in a variety of fields. Processing variables are also of great importance especially those concerned with raw materials and sintering [34].

A few years ago, we started our study of transparent ferroelectric ceramics, particularly of PLZT (lead lanthanum zirconate titanate) (Fig. 34). Two problems are of interest to us. The first is to study the degree of transparency with respect to the processing variables, including, in particular, the kind and activity of raw materials used and the influence of sintering (or hot-pressing) parameters [35]. The second is to study the relationship between microstructure and electro-optic properties [36]. Up to now, large sized plates with about 70%

TABLE X - Some properties of Si_3N_4 with no additive densified at super-high pressures.

Si_3N_4 material hot-pressed at	54 kilobar 1750°C	54 kilobar 1350°C	5% MgO 300 bar 1750°C
Bulk density, g/cm³	3.13	3.13	3.26
Main crystalline phase	β-Si_3N_4	α-Si_3N_4	β-Si_3N_4
Hardness, RA		—	91-92
Microhardness, Hv, kg/mm²	2220	—	1900
Microstructure	Finer and more uniform grain size distribution	Similar to 1750°C, 54 kilobar data	Coarser and less uniform distribution

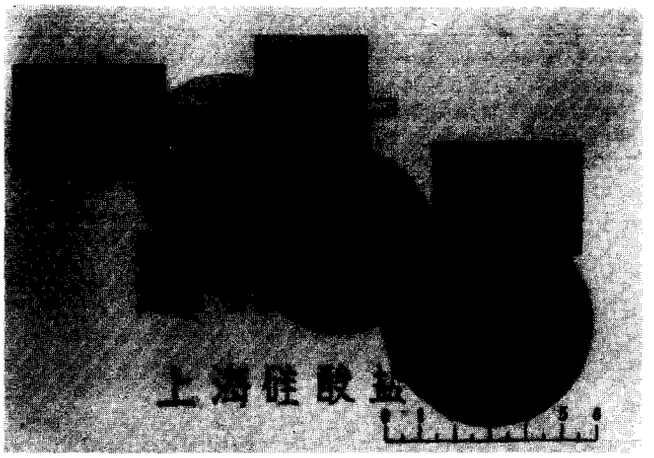

FIGURE 34 - Samples of transparent PLZT.

light transmittance can be regularly fabricated and quite good switching effect can be obtained with a proper bias field.

Fig. 35 shows a pair of transparent PLZT glasses inserted between crossed-Nicols. By electrically induced birefringence, the lenses can be turned on and off by applying or switching off an electric field. At the same time two TV cameras are focussing from slightly different angles on the same object and the images from these two monitors are superimposed on the same TV screen. A pulsed square wave modulation is then used to switch from one camera to the other and simultaneously from one of the lenses to the other, thus producing a quite good stereo image for the observer [37].

Because of its transparency, it can be used to study the effect of temperature, and of electric field on the dynamic change of electric domain [35]. For this purpose, we have developed a mono-grain thick polished slide technique for observation under an electric field or by the aid of a microphotometer. The samples to be observed can be specially cultivated to give a coarse grained microstructure, and electrodes are made by vapor deposition so that the direction of the applied field can be changed. Some interesting phenomena have been identified: (1) There is a « clean zone » near the grain boundary region of PLZT microstructure which does not easily etch (Fig. 36). This may indicate a region of higher strained state than the bulk. (2) When an electric field is applied, the PLZT crystal transforms from isotropic (« cubic ») to anisotropic (trigonal or tetragonal); thus it will turn bright under crossed Nicols. When the electric field is removed, the grains turn

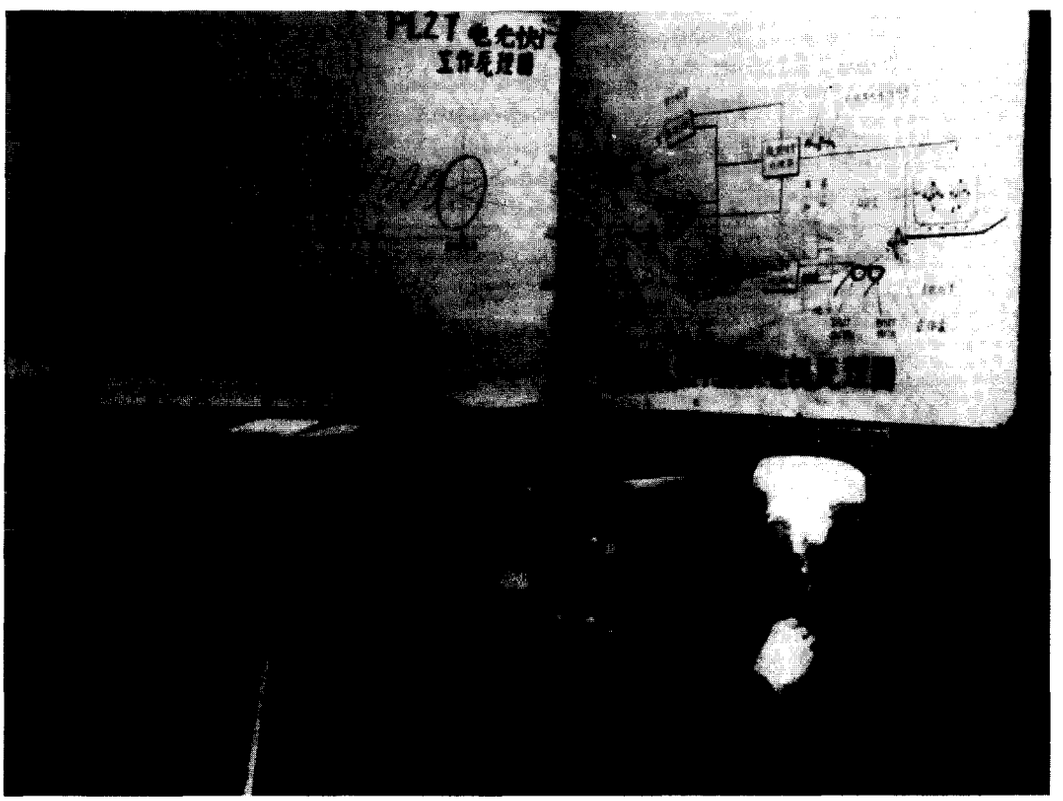

FIGURE 35
Principle of stereo VD by use of the electrically induced birefringence of PLZT glasses.

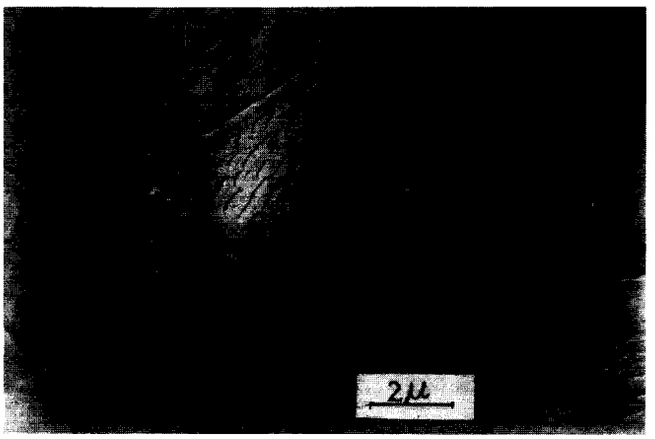

FIGURE 36 - « Clean region » near grain boundary of PLZT material (after thermal etching).

FIGURE 37 - « Wedge » domain shown originated from grain boundaries (↓), electric field 1000 V/mm, direction ↔.

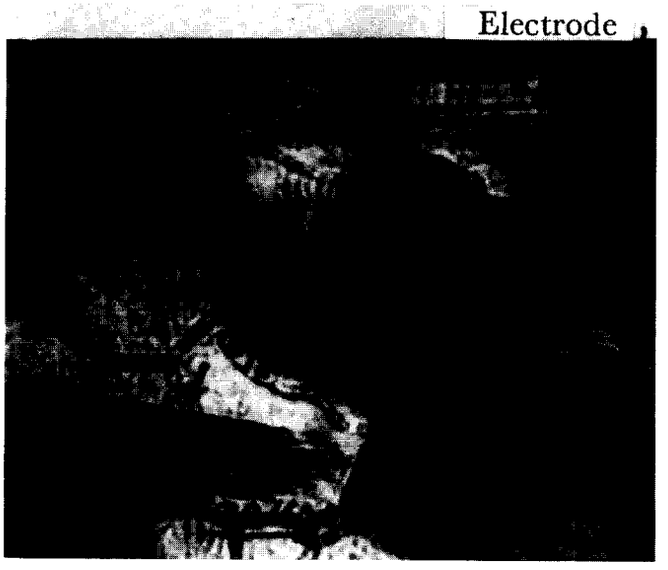

FIGURE 38 - Optical micrograph of domains extended across 2 or 3 grains, electric field 1000 V/mm, direction ↔ crossed Nicols.

dark again. But under this circumstance, the grain boundary region lags behind and remains bright. (3) « Wedge » domains can be seen to originate from the grain boundaries which indicate that these are more highly strained regions thus making easier the nucleation of electric domains (Fig. 37). Finally (4) some domains

FIGURE 39 - Domains discontinuous across grains.

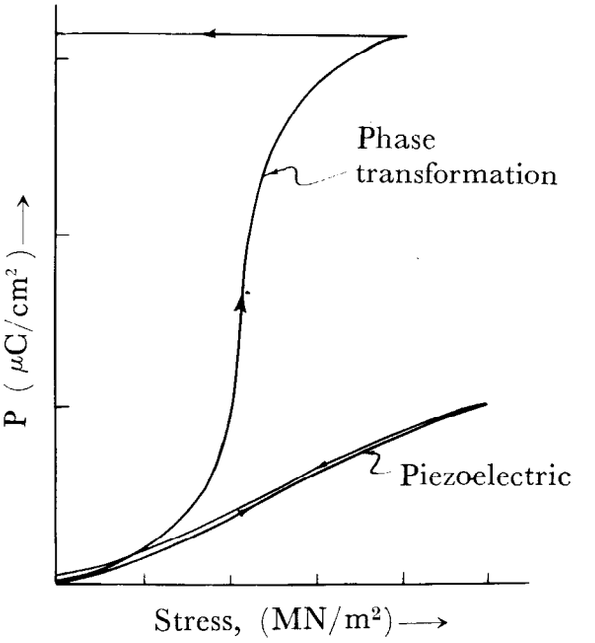

FIGURE 40 - Charge versus one dimensional stress of two PZT ceramics.

are seen to run through the boundaries of 2 or 3 grains (Fig. 38), while in others the domains are discontinuous across the grains (Fig. 39). This is an interesting method to study the dynamics of electric domains in relation to microstructure which can make them appear, change direction, or be erased.

Recently, we started to study a type of ferroelectric 95/5 PZT, which possesses an apparent electric or stress field induced phase transformation effect [38]. That is, under an electric field at room temperature, it transforms from an antiferroelectric to a stable ferroelectric phase. At the same time, it has a relatively high remanent polarization value (Pr) and relatively low dielectric constant.

By applying a stress field, if large enough, it will cause the reverse transformation to the antiferroelectric phase with a spontaneous release of electric energy. The charge release curve of such a system is nonlinear, and irreversible (Fig. 40) and thus differs from a typical piezoelectric material.

5 - STUDIES ON ANCIENT CHINESE POTTERY, PORCELAIN AND GLAZES

There are a few laboratories in China that have

been engaged in ancient Chinese porcelain and glaze studies from the technical and scientific aspects since the mid-fifties. We have an enthusiastic group in our Institute led originally by the former director Professor Zhou Jen that has done many beautiful pieces of work in this area. In this limited amount of space, I can try to introduce some of the highlights.

5.1 - Ancient Chinese pottery and its evolution into porcelain

From wares and sherds unearthed so far, pottery making in China may be traced back for about 10,000 years. Those that have been scientifically excavated and studied in detail include samples from Peiligang and Cishan of Honan Province, northern China [39] and those at Homudu, Zhejiang Province, southern China [40]. According to C^{14} dating, the ages are respectively 5195±300 B. C. and 5005±130 B. C. for these two places. The pottery wares excavated in the fourth cultural layer of Homudu, dating back about 7000 years, posses many distinguishing features. Large quantities of black pottery with included carbon were made of a kind of clay containing sericite and intentionally mixed with carbonized plant stalks and leaves (Fig. 41). From the variation in composition, firing temperature and the development of pottery making technique between the 4 different cultural deposit layers overlying one another at Homulu, a clear view can be obtained of the advancement of civilization 7000 years ago in the Yangtze valley; this is besides the one that has long been recognized at the Yellow river region up north.

FIGURE 41 - The microstructure of Homudu pottery (7000 years) with included carbonized material.

Studies of the sherds of black, white and colored pottery of the Yang-shao cultural (~3000 B. C.) and Lung-shan (~2000 B. C.) cultural periods [41] show that they are more varied in appearance and quite mature in pottery making. Firing temperatures reached 950-1050°C. For white pottery, porcelain clay had already been used. In the Yang-shao cultural period, potters wheel of the primitive stage had appeared and been used. The thin walled black pottery of the Lungshan period was really unique in its artistic level.

Besides studies of ancient pottery of the Neolithic age, all through these years, they have studied samples enearthed from more than one hundred localities and different historical periods from Shang, Zhou down to Sung, Ming, Qing covering some 3000 years [42, 43, 44, 45]. The gradual development of pottery through proto-porcelain to porcelain in China has been traced. They believe that the transition from pottery to proto-porcelain occurred during the Shang-Zhou period, about 3000 years ago. The light green glazed porcelain pieces unearthed at Zhang-Jia-po, Xian of West Zhou Dynasty (2600 years ago) already approached porcelain and were fired up

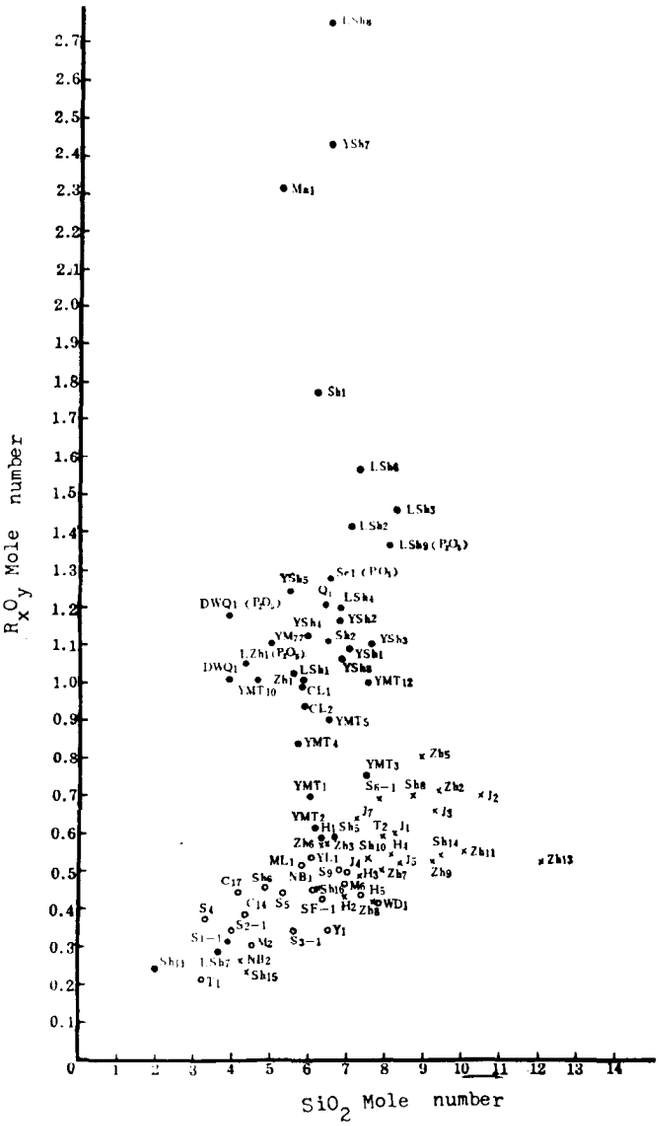

FIGURE 42 - The distribution of chemical composition of pottery and porcelain of different dynasties in China.
● - Pottery ○ - Porcelain X - Proto type porcelain
R_xO_y, Fe_2O_3, TiO_2, CaO, MgO, K_2O, Na_2O, MnO, P_2O_5.

to about 1200°C. Thereafter, until East Han Dynasty (about 2000 years ago), real porcelain came into its being. The celadon ware unearthed from the East Han kiln site at Shangyu, Zhejiang province is a good example [46]. It was already fired at about 1300°C. The micro-structure and physical-chemical properties of both the body and glaze approached those of present day porcelain ware [47]. Thus the progress from pottery to porcelain was realised, making China the first country to develop porcelain.

Based on their results, they pointed out that three essential break-throughs played significant roles in these changes or transitions [45, 47]: namely the selection and upgrading of raw materials; the improvement of kiln constructions and the increase of firing temperature; and, thirdly, the discovery and use of glazes. Fig. 42 shows the distribution of chemical composition of pottery and porcelain of the different periods. From Han, Jin and downwards, the compositions move gradually to the lower left corner of the figure with less SiO_2 and fluxes. The change in the iron content of pottery and porcelain of different dynasties is most important (Fig. 43). In pottery of neolithic age and Shang, Zhou, the Fe_2O_3 content usually amounts to 6% or above; this drops to around 3% in proto-porcelain, and then

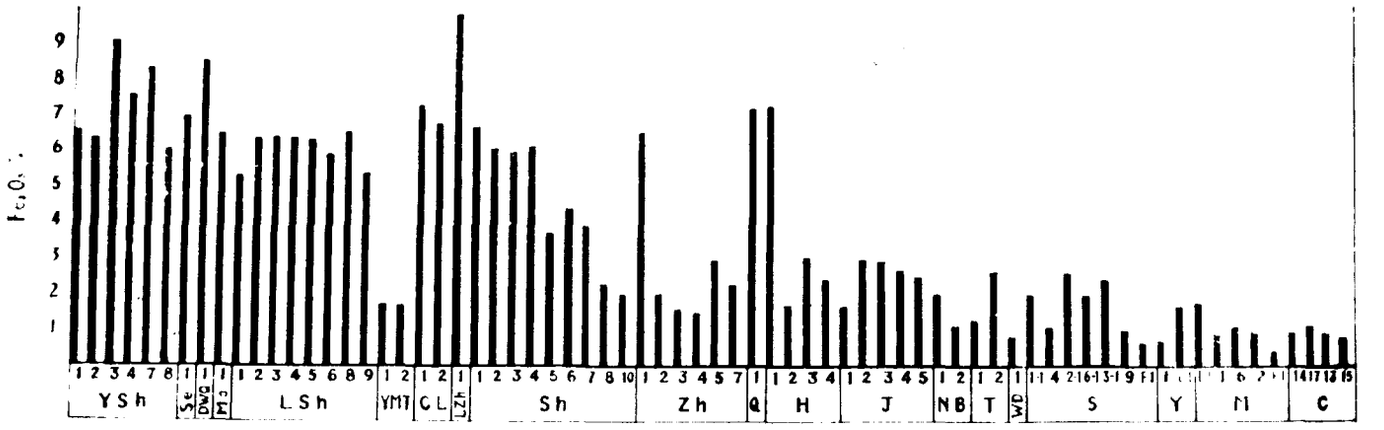

FIGURE 43 - The iron content of pottery and porcelain of different dynasties of China.

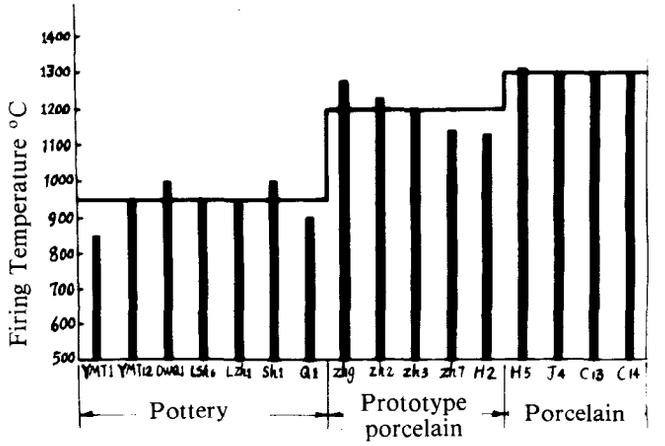

FIGURE 44 - The increase of firing temperature from pottery, proto-porcelain to porcelain through different dynasties.

further drops to about 1% in porcelains. The lowering of the Fe_2O_3 content is also one important cause of the fact that the firing temperature could be raised. The demarcations of firing temperatures between pottery, proto-porcelain, and porcelain of different dynasties are also rather clear and striking (Fig. 44).

5.2 - Famous Long-guan celadons and Jin-De-Zhen porcelain

Colouring with iron oxide and firing in reducing atmosphere to form celadon typed ware can be dated back to the East Han dynasty (25-220 A. D.)[46]. Celadons from Yueh Kiln, Zhejiang province, of that period[48] were shown to have been fired at 1260-1270°C with only some closed pores observed under the microscope and the bodies having apparent porosities of less than 0.5% (Fig. 45). These are considered to be high quality porcelains in view of their early appearance. The densification degree is not inferior to the celadons of the Tang, Sung and Five Dynasties.

The Long-quan celadons of the Sung Dynasty are world famous. Studies of Long-quan celadons of various periods[49] indicated that the body compositions are very close to those of Zhejiang China stone with intentional incorporation of a small amount of purple red clay (a high iron oxide clay) to give the celadons the typical charming and elegant touch, As to the glazes of Ge (Ko) type and De type celadons, they have different chemical compositions (De has slightly higher SiO_2 and CaO content) and are situated in different primary crystallization fields of the $CaO-Al_2O_3-SiO_2$ system. Thus the phase composition and the microstructure of these two types of glazes are entirely different. The De celadon glaze is typically glassy[49] (Fig. 46), with dispersed undissolved quartz grains and pores and some occasional anorthite crystals at the body-glaze interface. This microstructure causes the diffused effect on light beams that penetrate into the glaze, thereby producing a soft exquisite jade-like appearance. In contrast, the Ge type glazes are typically crystalline with prismatic plagioclase crystal clusters heavily dispersed in them[50] (Figs. 47, 48). The opalescent appearance and crackled nature of the Ge type glaze are believed to be mainly due to plagioclase crystallization. It has been found that there are also many scattering particles between the plagioclase crystals in the Ge type glazes (Fig. 49). Careful examination revealed that they are micropores of diameters less than 2000 Å which may contribute to light scattering at shorter wave length.

As a result of studies since the sixties[51, 52, 53], two varieties of De celadon and one variety of Ge ware have been revived their production after a break of more than two hundred years.

In respect to Jin-De-Zhen (Ching-Te-Cheng), this has long been a world famous porcelain production center. Since the founding of the People's Republic, studies have been carried out from the early fifties to understand technically and scientifically the nature of the porcelain produced in that area. It has been ascertained that the body is composed of the kaolin-quartz-sericite mica

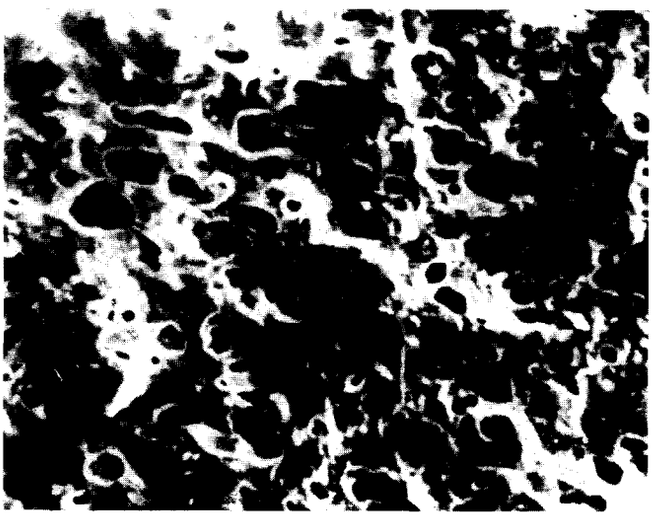

FIGURE 45 - Microstructure of Yueh Kiln celadon of East Han dynasty, fracture surface, SEM X 300.

FIGURE 46 - Microstructure of Long-quan celadon (De ware) of Southern Sung dynasty, X 120 (transmitted light).

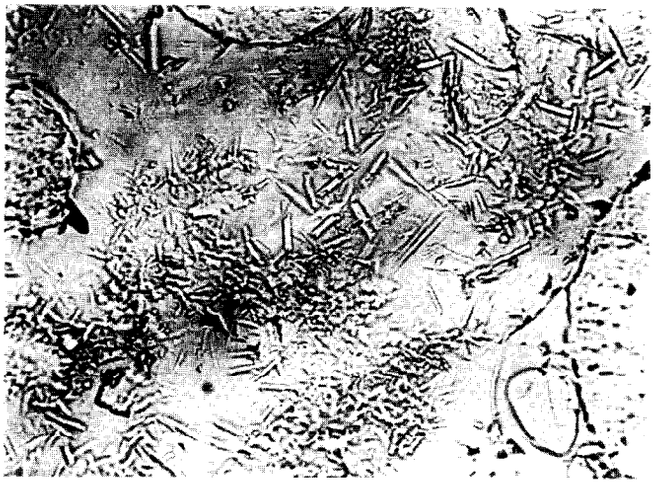

FIGURE 47 - Microstructure of Ge ware glaze excavated from the Great Capital of the Yuan dynasty, X 505 (transmitted light).

system and the glaze composed of the lime-quartz-sericite system [54]. Since the Five Dynasties and downwards, the Jin-De-Zhen body composition had gone through a gradual change [55]. In the earlier dynasties, essentially only china stone was used with a minor addition of kaolin. Gradually, more kaolin was incorporated (up to ~50%), thus the firing temperature was increased (to 1350°C) and the quality attained a higher level (Fig. 50). All the raw materials used in the preparation of Jin-De-Zhen porcelain contained some iron oxide and they were fired in a reducing atmosphere. Thus the Ching-Te-Cheng porcelain was famous for its « white tinted with light blue » traditional characteristics.

5.3 - Liquid phase separation in glazes

One of the most interesting findings recently with respect to glaze studies is the phenomenon of liquid phase separation and the most varied, exquisite and charming effects that may be brought about glaze appearance. Though liquid phase separation and immiscibility at high temperatures was observed some sixty years ago, but its existence in glaze structure was only speculated in recent years. The direct proof of such phenomena was only obtained very lately with the aid of modern electron microscopy techniques [56]. Such phenomena have since been identified in many other famous glazes; they are more common than expected and interesting indeed.

FIGURE 48 - Ge ware glaze of a sample from the Imperial Palace, X 500 (transmitted light).

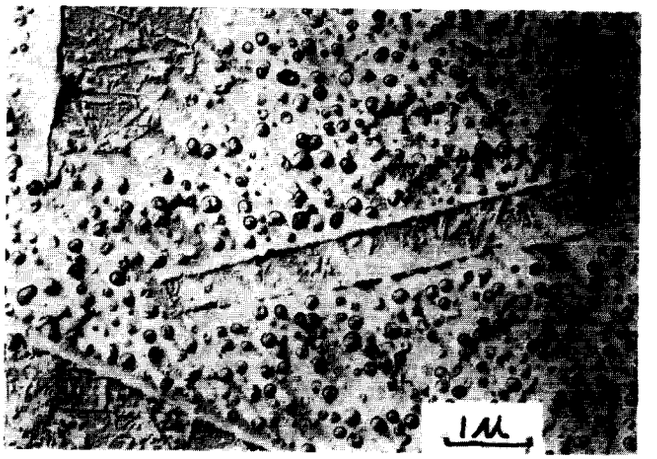

FIGURE 49 - Electron micrograph of Ge ware glaze from the Great Capital of the Yuan dynasty, polished section, not etched.

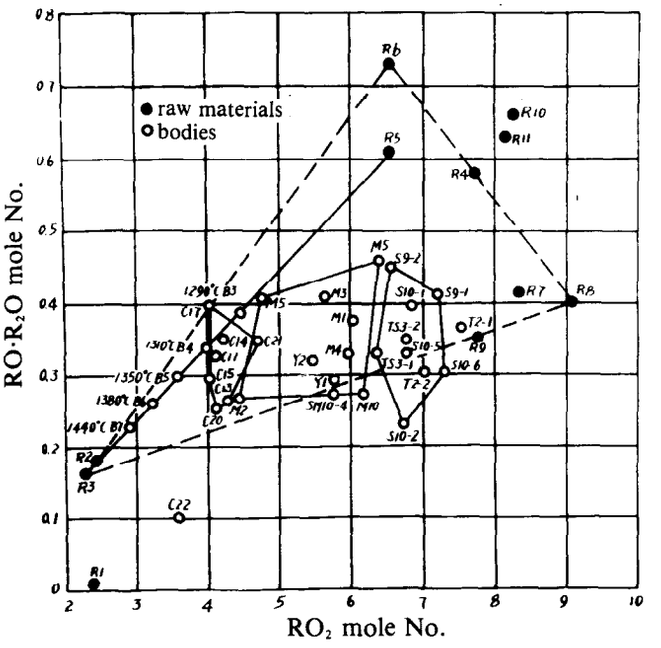

FIGURE 50 - The variation of composition and firing temperature of Jin-De-Zhen (Ching-Te-Cheng) porcelain.

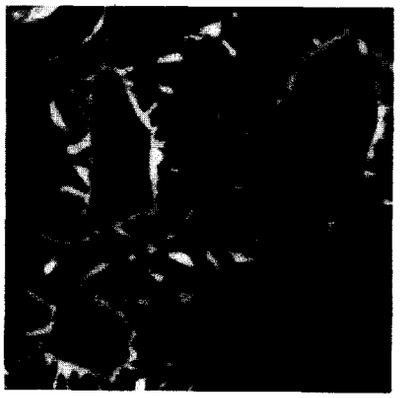

FIGURE 51 - Microstructure of Jun sample, cristobalite crystallization around quartz grains, X 630, phase contrast.

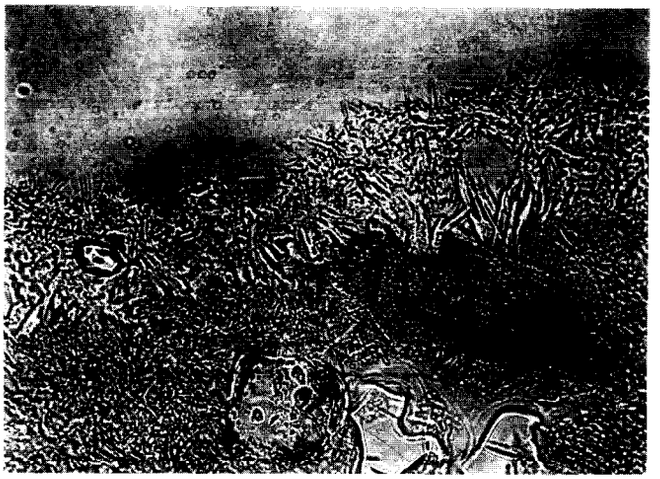

FIGURE 52 - Microstructure of Jun sample, crystallization of anorthite and plagioclase crystals at the body-glaze interface, X 478, transmitted light.

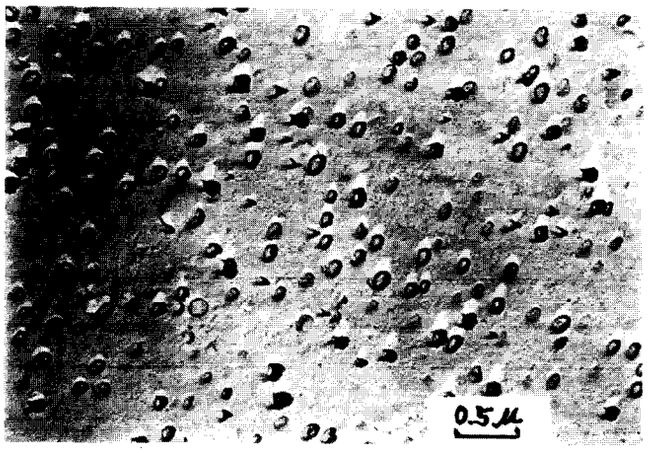

FIGURE 53 - Electron micrograph of Jun glaze, showing micropores in the blue glaze region.

5.3.1 - Jun (Chün) ware glaze of the Sung and Yuan dynasties

Sung Jun ware of Honan province has a typical sky blue opalescent appearance with purplish red spots. As to the area of red dots, besides containing some CuO (<0.5%), it has no difference in chemical composition from that of the sky blue areas.

Microstructure studies revealed that ancient Jun ware possesses many unique structural characteristics [57] as seen in Figs. 51 and 52. Besides, large amounts of micropores with sizes of about a few thousand angstroms

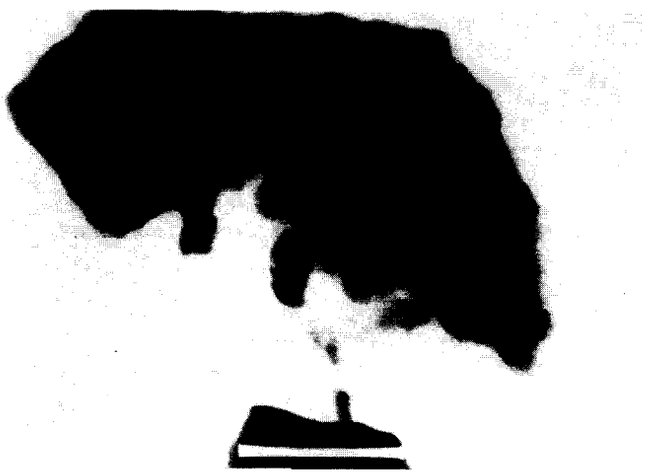

FIGURE 54a - Micrograph of the red spot, in Jun glaze HVEM, 1000 kV, Label 0.5 μm.

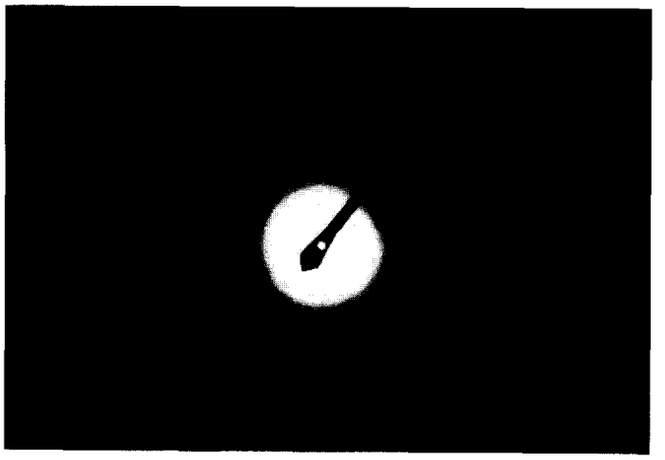

FIGURE 54b - In-situ electron diffraction of a droplet, same Jun glaze.

FIGURE 55 - Jun glaze, smaller liquid droplets in the blue area, HVEM, 1000 kV.

were seen to be separated out in the glaze (Fig. 53).

Even more exciting is the direct proof by high voltage electron microscopy (1000 kV) that liquid phase separation exists in both the sky blue and reddish spot areas [58]. HVEM observations of thin flakes of the glazes under 1000 kV show unequivocally the existence of two immiscible liquid phases and in-situ electron diffraction proved that the droplets are amorphous — not crystallized even after some 900 years (Figs. 54a, b). The droplets in the red spot areas are larger with

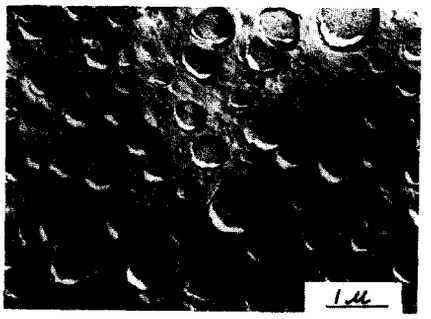

FIGURE 56 - Electron micrograph of Jian-yang Hare's fur showing liquid-phase separation structure.

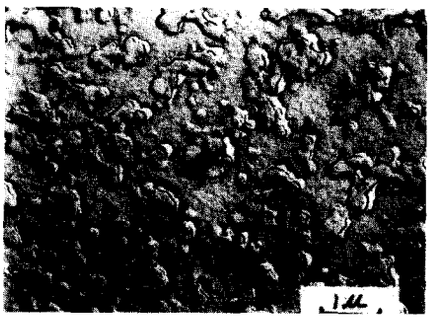

FIGURE 57a - Ji-zhou Tortoise shell, showing its two-phase microstructure.

FIGURE 57b - Ji-zhou Tortoise shell, showing its two-phase microstructure.

usual diameters of 1000-1500 Å. Those in the blue glaze areas are smaller, usually 500-800 Å, with smaller ones even ≤400 Å (Fig. 55).

5.3.2 - Sung Tian-mu (Temmoku) glazes

The black glazed Tian-mus (or Temmoku) of the Jian-yang area from the North Sung dynasty are world famous. Recently, we have collected famous ancient Tian-mu sherds from different localities. Nine of these samples including Jian-yang Hare's Fur, Ji-zhou Tortoise shell, Ji-zhou Yohen, Shan-xi Silver Oil Spot and Shan-xi Red Oil Spot, have Fe_2O_3 content 4-6%, CaO 6-9%, P_2O_5 content usually above 1%, some even approaching 2%. By our experience, glazes with some P_2O_5 content easily develop a phase separation microstructure. By studying these samples, my colleagues discovered, for the first time, that liquid-phase separation phenomena exist in Jian-yang Hare's Fur, Ji-zhou Tortoise Shell and Shan-xi Red Oil Spot specimens [59].

For the Jian-yang Hare's Fur sample, the size of isolated droplets near the fur's hair are large enough to be identified by optical microscopy pushed to its ultimate resolution. Electron micrograph confirms that these droplets are below 1 μm in size (Fig. 56).

For the Ji-zhou Tortoise Shell sample, some droplets are connected together in threes and fours, even forming an interconnected two-phase structure (Figs. 57a, b). This, in some way, is similar to a spinodal decomposition microstructure.

For the Shan-xi Red Oil Spot specimen, well-developed anorthite needle crystals forming the bone-structure of the red spot are clearly seen. In between are relatively well grown magnetite crystallites. Around the bone structure, there are the two liquid, phase separated, areas. The microstructure has scales large enough to be resolved clearly by an optical microscope (Fig. 58).

These results will help to indicate how iron containing black glazes of Tian-mu (Temmoku) could have changes of a thousand varieties.

Jian-yang Hare's Fur was lost for several hundred years. The Jian-yang district of Fujian province is now trying to revive this famous ware and has already made good progress. The duplicates have similar micro-structure to the ancient pieces.

5.3.3 - Complicated liquid-phase separation in contemporary iron oxide red glaze

We have studied a contemporary iron red glaze produced by our porcelain capital Jin-De-Zhen. The glaze of the ware has a sea cucumber brown background with red flowers spread on it. This is a silicate glaze with high P_2O_5 (~7%) and Fe_2O_3 (~12%) content. Investigation of its microstructure revealed that extensive

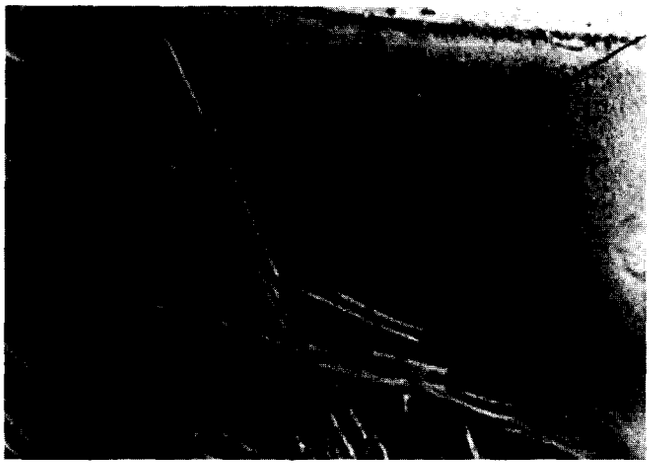

FIGURE 58 - Optical micrograph of Shan-xi Red Oil Spot Glaze, showing its complicated microstructure, X 640.

FIGURE 59 - Liquid-phase separation in iron red glaze, transmitted light, oblique illumination X 1500.

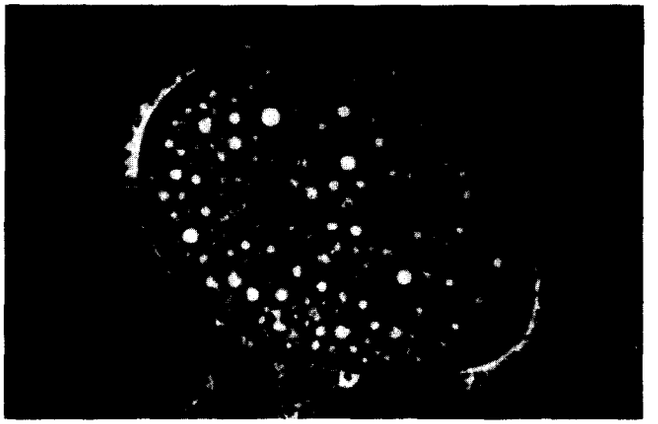

FIGURE 60 - Secondary phase separation seen in the elliptical area, transmitted light, X 742.

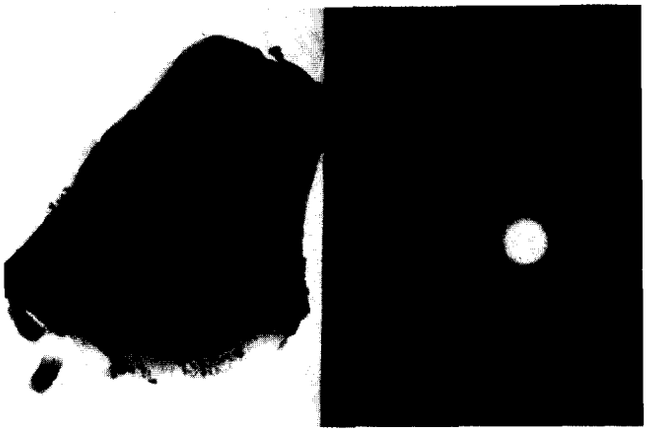

FIGURE 61 - Iron red glaze showing α-Fe_2O_3 precipitation by ED, TEM, 200 kV, X 36000.

liquid-phase separation is prevailing in this type of glaze [56, 60]. Primary phase separation, resulting a microstructure having a large number of iron rich droplets dispersed in a relatively iron poor matrix, forms the brown background of the glaze (Fig. 59). In certain areas, especially near the glaze surface, the iron rich droplets coalesce and form big drops in which secondary phase separation may occur, Fig. 60 shows the microstructure of such an area, in which iron poor drops are seen dispersed in an iron rich continuous matrix. The iron rich matrix then precipitates out α-Fe_2O_3 crystallites forming the red flowers. Electron diffraction gives such evidence (Fig. 61). All these processes of phase separation, coalescence, secondary phase separation and crystallization happen during cooling in the temperature range of about 1260-1000°C. Of course the cooling rate is a kinetic factor which must also be of importance to give the elegant artistic touch as desired. Composition and processing variations can result in a wide variety of patterns and this is certainly an interesting problem to go into.

The identification of such a multiplicity of liquid phase separation phenomena in such a variety of ancient and modern glazes is unique.

ACKNOWLEDGEMENT

This review has given a brief account of some of the main works that have been done or are going on in our Institute. In the last few years, we have enjoyed quite a number of contacts with scientists of many other Countries. It is hoped that this review will promote further understanding and foster increasing collaboration between us and colleagues of other Countries in this branch of materials research. To this end, I would like to extend my sincere acknowledgement to the General Editor of Ceramics International for offering me this opportunity.

REFERENCES

1. ZHONG WEI-ZHUO, Acta Physica Sinica **28** (1979) 240.
2. ZHANG YUAN-LONG, Acta Physica Sinica **28** (1979) 40.
3. C.F. HE, P.J. LI and Y. ZHAN, Kuxeutungbo (1965) 457.
4. C.F. HE, Nature Magazine (China) **2** (1979) 615.
5. FAN SHI-JI, Jour. Chinese Silicate Society **8** (1980) 1.
6. Artifical Diamond, (in Chinese), **15** (1975) 9.
7. Z.D. QI, Z.Q. YANG and Z.J. CAO, New Inorganic Materials, (in Chinese, an interim publication by the Shanghai Institute of Ceramics), **6** (2) (1978) 8.
8. R.Y. XU, Q.B. ZHU et al., Special Report on Chinese Crystal Growth and Materials Conference (1979).
9. X.S. ZHANG et al., New Inorganic Materials (in Chinese) **5** (2) (1979) 9.
10. X.S. ZHANG et al., New Inorganic Materials **7** (3) (1979) 21.
11. J.M. LIN et al., Shanghai Inst. of Ceramics Report (1980).
12. H.Y. TAN et al., Shanghai Inst. of Ceramics Report (1981).
13. H.F. WU, H.D. XU, Shanghai Inst. of Ceramics Report (1981).
14. X.M. HE et al., Laser (in Chinese) **7** (4) (1980) 26.
15. Z.Q. BAO, J.Z. LI, C.D. SHEN, Jour. of Chinese Silicate Society **9** (1) (1981) 1.
16. Q. TENG, P.W. NI and Y.H. ZHANG, Jour. of Chinese Silicate Society **8** (4) (1980) 357.
17. S.Q. MIN, H.M. YANG, X.H. GAO and W.Z. WANG, First National Conference on Amorphous Solid, China, (1978).
18. H.M. YANG et al., Jour. of Chinese Silicate Society **8** (3) (1980) 270.
19. G.C. ZHANG, X.X. CHENG et al., Jour. of Chinese Silicate Society **8** (1) (1979) 11.
20. D.H. WU, J.F. CHENG and S.Q. MIN, Wu Li, ibid., (in Chinese) **9** (5) (1980) 383.
21. T.S. YEN et al., Special Publ. of the Inst. of Metallurgy and Ceramics, Academia Sinica, (1958).
22. R.L. COBLE, J. Appl. Phys. **32** (1961) 787, 793.
23. R.L. COBLE, U.S.P. 3026210, (1962).
24. T.S. YEN, Kuxeutungbo (A monthly scientific journal), (1964) 682.
25. W.L. LI, Shanghai Institute of Ceramics Report, unpublished. (1980).
26. G. KWAN, S.H. TAN and J.H. WANG, New Inorganic Materials, **8** (2) (1980) 75.
27. X.X. HUANG et al., New Inorganic Materials **5** (1) (1977) 13.
28. L.P. HUANG, W.L. XUE and M.Z. LI, Jour. Chinese Silicate Soc. **7** (4) (1979) 346.
29. Y.T. CHEN, F.Y. WU and T.S. YEN, Shanghai Inst. of Ceramics Report, to be published (1980).
30. S.L. WEN, D.A. JEFFERSON and J.M. THOMAS, work done in Cambridge University in Collaboration with the Shanghai Institute of Ceramics, Academia Sinica, to be published (1980).
31. T.G. XI et al., to be published (1980).
32. W.L. LI and L. YU, New Inorganic Materials **7** (3) (1979) 61.
33. Y.Y. GUO, Q. CUI et al., New Inorganic Materials **2** (4) (1973) 38.
34. Y.K. LU, Y.W. YANG and H. WANG, New Inorganic Materials **6** (1) (1978) 61.
35. B.H. CHU, R.M. SUN and C.W. YIN, Proc. International Symposium of Factors in Densification and Sintering of Oxide and Nonoxide Ceramics (1978) Japan pp. 601-609.
36. B.H. CHU, H.K. NGAO and Z.J. GU, Proc. IMF-4 (1979) p. A5.
37. W.G. LUO and A.L. DING, New Inorganic Materials **7** (4) (1979) 32.
38. Y.L. WANG, C.W. LIN et al., Shanghai Inst. of Ceramics Report, (1981).
39. Z.M. AN, Archaeology (4) (1979) 335.
40. J.Z. LI, H.Q. CHEN, Z.Q. DENG and Z.J. GU, Jour. Chinese Silicate Soc. 7 (2) (1979) 105.
41. J. CHOU, F.K. ZHANG and Y.F. ZHEN, The Chinese Jour. of Archarology (1) (1964) 1.
42. J. CHOU, J.Z. LI and Y.F. ZHEN, Archaeology (9) (1960) 48.
43. J. CHOU, J.Z. LI and Y.F. ZHEN, ibid (8) (1961) 444.
44. J.Z. LI, Bull. Chinese Chemical Soc. (6) (1977) 362.
45. J.Z. LI, Archaeology (3) (1978) 179.
46. B.C. CHU et al., Jour. Chinese Silicate Soc. **6** (3) (1978) 220.
47. J.Z. LI, ibid. **6** (3) (1978) 190.
48. Y.Y. GUO, S.Y. WANG and Y.C. CHEN, Jour. Chinese Silicate Soc. **8** (3) (1980) 232.
49. J. CHOU, F.K. ZHANG and Y.F. ZHEN, The Chinese Jour. of Archaeology (1) (1973) 131.
50. H.Q. CHEN, J.Z. LI and R.F. HUANG, Jour. Chinese Silicate Soc. **8** (2) (1980) 147.
51. J. CHOU, Y.Y. KUO and M.Y. WAN, unpublished work.
52. H.M. YE and C. LI, unpublished work.
53. K.C. LI and H.M. YE, Jour. Chinese Silicate Soc. **3** (1) (1964) 1.
54. J. CHOU, Y.Y. GUO and J.Z. LI, Special Report, Institute of Metallurgy and Ceramics, Academia Sinica, (1958).
55. J. CHOU and J.Z. LI, Jour. Chinese Silicate Soc. **4** (2) (1960) 49.
56. H.Q. CHEN, R.F. HUANG, S.P. CHEN, D.F. CHAO and J.T. WANG, Porcelain (3) (1979) 1.
57. H.Q. CHEN et al., to be published (1980).
58. H.Q. CHEN, R.F. HUANG, S.P. CHEN and M.L. YUAN, New Inorganic Materials (2) (1980) 165.
59. H.Q. CHEN, R.F. HUANG, S.P. CHEN and M.L. YUAN, The Shanghai Institute of Ceramics Report, to be published, (1980).
60. H.Q. CHEN, R.F. HUANG, S.P. CHEN and M.L. YUAN, Porcelain (4) (1980) 48.

Received 1981; accepted July 6, 1981.